Performance Analysis of a Compact UHF RFID Ceramic Tag in High-Temperature Environments

A. Ria, *Student Member, IEEE*, A. Michel, *Member, IEEE*, R. K. Singh, *Student Member, IEEE*, V. Franchina, P. Bruschi, and P. Nepa, *Senior Member, IEEE*

***Abstract*— In this paper an experimental analysis of the effect of high temperature on the performance of a compact UHF RFID tag is described and discussed. The tag is designed to be integrated into small cavities carved out of metal objects to identify themselves during the entire fabrication and assembly line. Since the UHF RFID tag is applied just after the die casting operations needed to model the metal component, it must be robust to high temperature manufacturing environments and processes. Tests demonstrated a significant chip input impedance variation by increasing the surrounding temperature, with a consequent read-range reduction. However, the considered ceramic tag can be detected at a satisfactory distance of 30 cm when employed with temperatures so high as up to 120 °C.**

***Index Terms*— Die casting, high-temperature, in-metal tag, metal embedded tag, Tag antenna, UHF RFID.**

I. Introduction

Nowadays, it is a common place to recognize to the Radio Frequency Identification (RFID) technology a key role in industrial applications such as the inventory and tracking of goods in supply chain. For example, Ultra-High Frequency (UHF) RFID systems are suitable for low-cost but long read range applications such as electronic toll collection, waste management, animal tracking, IoT-based personal healthcare, vehicle monitoring, remote monitoring of human subjects, bike tracking, item level tagging, smart shelf [1], [2].

A focus of interest is the use of UHF RFID system to identify and track small metal components needed to assembly more complex systems. As an example, in the last years, Air bus and Boeing proposed the use of RFID tags in identifying commercial aircraft parts, and RFID-enabled aircraft maintenance systems were designed [3]. In particular, in [4] it has been demonstrated that by wirelessly collecting information stored on the RFID tags applied to each parts, it is possible to develop an RFID-based configuration control system to improve the health monitoring of aircraft landing gears. Likewise, the identification of metal parts of cars, trains and industrial machineries may be of interest during the assembly process.

It is worth noting that some of the metal components are customized and their shapes are obtained after a die casting process or by means of metal 3D printers. In both cases, the UHF RFID tag is required to withstand to high temperature in order to be applied to each item immediately after the metal component fabrication and shaping. Moreover, in order to use the same tag for a large number of metal components, the latter should be as small and compact as possible, and preferably it should be integrated into small cavities carved out of the metal component, so preventing protrusions on the component surface. For these reasons, metal-attachable compact tags have been proposed in the scientific literature [5]-[14].

The most common antenna layout considered for UHF RFID on-metal tags are inverted-F antenna, planar inverted-F antennas (PIFA) and patch-like structures [5]-[8]. In [9], [10] examples of small and flexible metal mountable UHF RFID tags were described, while in [11], [12] loop-type antennas have been considered. Recently, in [13], the authors have proposed a low-profile in-metal tag designed to be embedded in thin cavities carved out of small metal parts. The proposed tag consists of two miniaturized quarter-mode patch antennas properly arranged to make the tag less sensitive to the presence of the cavity metal walls. The presence of a commercial epoxy resin is considered during the design process and exploited to reduce the tag antenna physical size. Both simulated and measured performance are discussed in [13], [14]. As discussed in [15]-[19] for both HF and UHF RFID tags, the temperature variation may affect the chip and tag performance. In [16], the authors studied the performance and reliability of passive inexpensive RFID tags in high temperature cycling test (20-180 °C) combined with water immersion; humidity effects have also been investigated. The functionality of the RFID tags was monitored regularly after certain test periods with threshold power measurements. Results showed that high temperature cycling tests, alone and also combined with water immersion prior to the cycling test, did not have a detrimental effect on reliability (only few intermittent failures were detected). When the samples were immersed in water, between the cycling test periods, reliability decreasing was observed. In [17], sensing and communication

Manuscript received XXX

Work partially supported by the Italian Ministry of Education and Research (MIUR) in the framework of the CrossLab project (Departments of Excellence).

A. Ria (*corresponding author*), A. Michel, R. K. Singh, V. Franchina, P. Bruschi and P. Nepa are with the Department of Information Engineering, University of Pisa, 56122 Pisa, Italy (e-mail: andrea.ria@ing.unipi.it, andrea.michel@unipi.it,rajesh.singh@dii.unipi.it, vittorio.franchina@ing.unipi.it, paolo.bruschi@unipi.it, paolo.nepa@unipi.it).

performance of three kind of RFID tags under high temperature stress were experimentally investigated by means of an RFID reader close to the tags heated by an electric oven. The experimental analysis verified the degradation of the sensitivity for some popular RFID microchips exposed to high temperature exceeding the operating temperature recommended on datasheet, showing that tags were not responding once temperature reached ~150°C. Also, the reversibility of the reading process has been demonstrated, and tags were reactivated again once temperature dropped below the threshold level (close to 145°C). In [18], survivability of 13.56 MHz RFID tags attached to the blood bags has been measured after exposure to centrifugation, blast freezing and gamma radiation. The obtained results concluded that the mentioned processes have no significant impact on HF-RFID tag performance. Statistically, significant degradation is observed for mean time to read and write all blocks mainly after the thawing cycle. However, the time taken to read and write was within the acceptable threshold. In [19], a temperature control system to study the influence of temperature on the RFID tag's dynamical reading performance has been described. The reading distance of the tag has been measured by varying the temperature from 20°C to 70°C; it was showed a deterioration in the read distance with increase in temperature.

In this work, the effects of high temperatures on the tag performance have been investigated. Specifically, the UHF RFID chip input impedance variation by changing the temperature has been experimentally assessed, which affects the matching between the chip and tag antenna. Moreover, by taking into account the in-metal UHF RFID tag proposed in [13], [14], read range measurements have been carried out while heating the UHF RFID tag, also monitoring the activation power variation versus the temperature. As demonstrated in the preliminary results presented in [15], such an analysis is suitable to justify the UHF RFID system performance degradation when employed in high-temperature environments.

II. An in-Metal Compact Tag

The UHF RFID tag described in [13], [14] is designed on a 1mm-thick alumina (Al_2O_3) substrate (ε_r=9, tanδ=0.0003) and it consists of two miniaturized quarter-mode patch antennas. The layout of the antenna is shown in Fig. 1(a). The antenna has been accommodated in a $L_C \times L_C \times H_C$ cavity carved out of the 150×150×7 mm^3 metal object and then covered by a H_R=1.5mm thick epoxy resin (ε_r=4.8, tanδ=0.015) [20]. As discussed in [13], the cavity size is required to be as small as possible, so that it can be etched also on small metal objects. On the other hand, antenna size can not be arbitrarily small, since its radiation efficiency reduces with the size, thus limiting the read range. Moreover, a distance between cavity lateral walls and antenna edges must be guaranteed to avoid short circuits between the top and the bottom layers of the tag. The final size of the cavity ($L_C \times L_C \times H_C$) is a trade-off between tag antenna performance and compactness of the cavity. The main antenna parameters are shown in Fig. 1 and their values are listed in Table I.

The meanders in the resonating edges are effective in reducing the electrical size of the antenna and can be fine-tuned to optimize the antenna performance. The tag antenna consists of two quarter-wavelength patch antennas radiating from the central slot between them, so limiting the effect of the cavity walls. Based on the numerical results obtained by means of the commercial software CST Microwave Studio®, the cavity size L_C has been set to 25mm. A smaller cavity may significantly affect the tag performance.

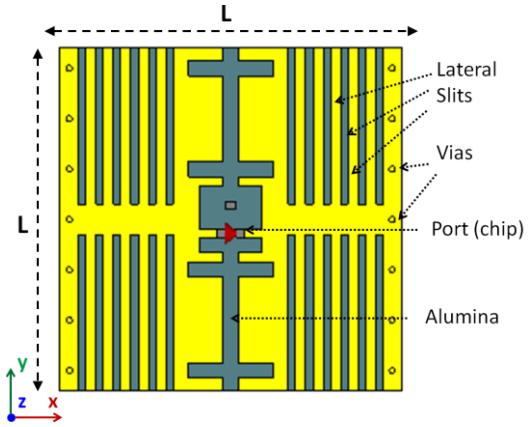

(a)

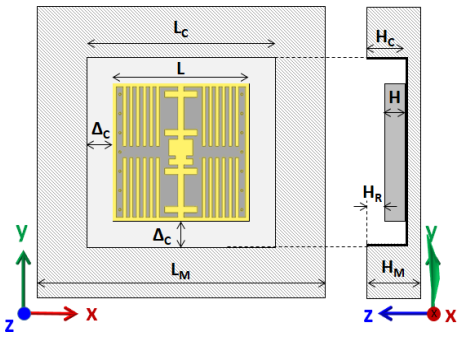

(b)

Fig. 1. Structure of the simulated antenna: (a) 3D view of the antenna in free space and (b) front and lateral view of the antenna embedded in a metal cavity [13].

TABLE I. ANTENNA MAIN PARAMETERS

Parameter	VALUE	PARAMETER	VALUE
L	23mm	Δ_C	1mm
H	1mm	L_C	25mm
L_M	150mm	H_C	2.5mm
H_M	7mm	L_S	11mm

In particular, the simulated antenna has been optimized to match the input impedance of the commercial RFID chip EPC Global Class-1 Gen-2 Higgs 4 IC with the standard SOT323 package. This chip is manufactured by Alien Technology [21]. As stated in [21], the equivalent circuit of the Alien Higgs 4 chip consists of a parallel connection of a capacitor (C=0.95pF) and a resistor (R=1.8KΩ). Thus, the nominal chip impedance at the room temperature corresponds to Z_{IC} = 20.55–j191.25 Ω at the ETSI UHF RFID central frequency (i.e. 866 MHz). As it is also described in [11], to achieve a low reflection coefficient, the antenna impedance Z_{in} must be approximately the complex conjugate of Z_{IC}. Hence, antenna layout has been optimized to achieve an input impedance value close to Z^*_{IC}. In Fig. 2, the antenna input impedance is plotted as a function of the frequency. The simulated value of input impedance is $Z_{in} \cong 10.3+j189\ \Omega$ at the ETSI UHF RFID central frequency. Moreover, in Fig. 3, the antenna radiation patterns on the two principal planes (i.e. E-plane, H-Plane) are shown.

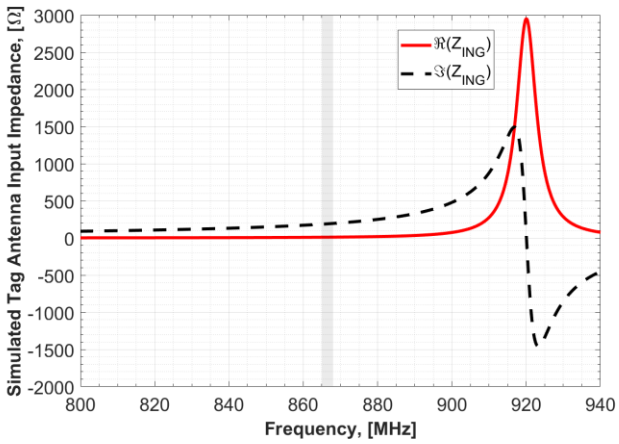

Fig. 2. Simulated real and imaginary parts of the input impedance when the tag is placed inside a 25×25×2.5 mm^3 cavity and covered by an epoxy resin (ε_r=4.8, tanδ=0.015).

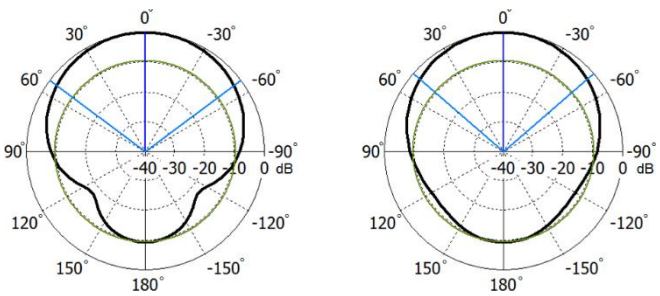

(a) (b)

Fig. 3. Simulated radiation pattern at 866 MHz on (a) X-Z plane (E-plane) and (b) Y-Z plane (H-plane) when the tag is placed inside a 25×25×2.5 mm^3 cavity and covered by an epoxy resin (ε_r=4.8, tanδ =0.015).

By using the equation (1) it is possible to estimate the tag read range as

$$R_{read} = \frac{c}{2\omega}\sqrt{P_{tx,EIRP} \cdot D_{tag} \cdot \eta_{tag} \cdot \frac{\tau}{P_{IC,sens}}} \qquad (1)$$

where c is the speed of light, $P_{tx,EIRP}$ is the equivalent isotropic radiated power of the reader device, D_{tag} and η_{tag} are the directivity and radiation efficiency of the tag antenna, respectively. $P_{IC,sens}$ is the reading sensitivity of the microchip, i.e. -18.5 dBm. The Power Transmission Coefficient, τ, is defined as in equation (2),

$$\tau = 4\frac{R_{chip} \cdot R_{tag}}{\left|Z_{chip} + Z_{tag}\right|^2} \qquad (2)$$

where $Z_{tag} = R_{tag}+jX_{tag}Z_{TAG} = R_{TAG} + jX_{TAG}$ and $Z_{chip} = R_{chip}+ jX_{chip}Z_{CHIP} = R_{CHIP} + jX_{CHIP}$ represent the tag antenna input impedance and the Alien Higgs 4 IC input chip impedance, respectively. In Fig. 4 the estimated read range computed by using (1) is plotted as a function of the frequency, demonstrating that the 23×23×1 mm^3 tag optimized in a 25×25×2.5 mm^3 metal cavity and with a H_R=1.5mm thick epoxy resin superstrate can read up to 1.5 m at the UHF RFID ETSI band (*Config A*). However, the absence of the resin leads to a shift of the maximum read range toward higher frequencies, thus significantly deteriorates the performance at the UHF ETSI band (*Config B*). Specifically, the read range drops to less than 30 cm when the epoxy resin is removed. A slightly better performance is obtained when the uncovered tag is placed on metal (*Config C*), but it still may not be satisfactory for a practical application. A preliminary experimental validation of these results can be found in [22].

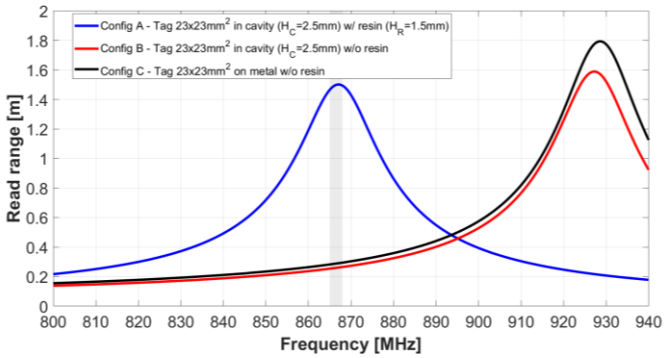

Fig. 4. Simulated read range as a function of the frequency for the 23×23×1 mm^3 tag in three configurations: the tag placed inside a 25×25×2.5 mm^3 cavity carved out of a metal plate (150×150×7 mm^3) and covered by an 1.5mm-thick epoxy resin (ε_r=4.8, tanδ=0.015) (Config A); same configuration as Config A but without resin (Config B); same configuration as Config A but on metal and without resin (Config C).

Another parameter that is generally used by antenna designers is the Power Reflection Coefficient (PRC), as defined in equation (3) [13]. This term quantifies the matching between the antenna input impedance and the chip impedance, and it can be used instead of the Power Transmission Coefficient (τ), by analogy with the reflection coefficient typically used by antenna designers. Typically, a PRC lower than -3dB is required to guarantee a satisfactory read range [13].

$$PRC = 1-\tau = 1-4\frac{R_{chip} \cdot R_{tag}}{\left|Z_{chip} + Z_{tag}\right|^2} \qquad (3)$$

It is well known that both the chip and the antenna input impedance depend on the frequency. However, they also depend on the operating temperature, and may represent key parameters when the RFID system is employed in high-temperature scenarios. In a first analysis, we can neglect the effect of the temperature on the antenna input impedance because the maximum considered temperature (130°C) is lower than the substrate glass transition temperature (180°). Nevertheless, the chip input impedance is more affected by temperature.

III. Experimental Assessment

The effect of temperature on the chip input impedance has been investigated by means of an ad-hoc calibration kit. In this Section, the measurement setup as well as the experimental results are described and discussed in detail. Moreover, a system-level analysis of the temperature on the achievable read range is described.

A. Effect of the Temperature on the Chip Input Impedance

An ad-hoc calibration kit has been fabricated to measure the chip input impedance by means of a Vector Network Analyzer (Agilent E5071C). In Fig. 5, the custom printed circuit board (PCB) is shown. It was designed with KiCad free software and

fabricated by means of a consolidated production stream of FR4 substrate suitable for high temperature applications (higher than 140 °C) and the copper layers thickness was of 35 µm.

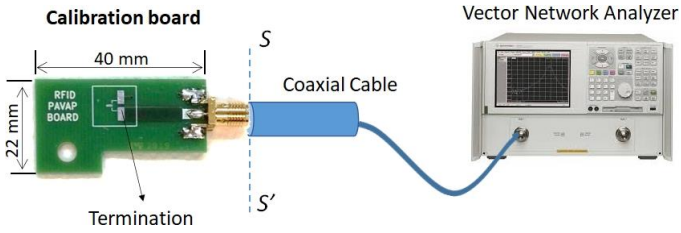

Fig. 5. Schematic representation of the calibration setup with a photo of the customized FR4 board. The dimensions of the calibration board are highlighted.

The calibration setup is schematically shown in Fig. 5. Before measuring the chip input impedance at different temperatures, the system has been calibrated at the *SS'* section by using the calibration kit of the VNA.

Three replicas of the same PCB were used to perform the calibration phase with three different terminations conditions (i.e. open, short, load), as suggested in [23], [24]. For the load condition, we soldered a 50Ω SMD resistor between the pads. In a similar way, to obtain the short condition, a copper wire was soldered. Measured S_{11} parameters of the three calibration boards are represented on a Smith Chart in Fig. 5.

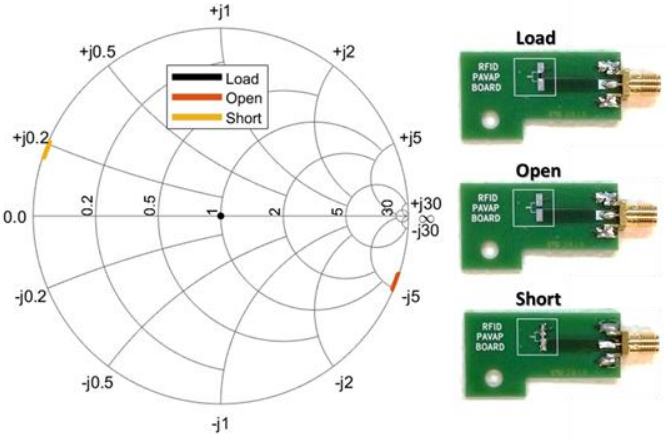

Fig. 6. Measured S_{11} parameter as a function of the frequency (range 800-1000 MHz) for the three terminations: load, open and short.

As shown in Fig. 5, even though the length of the microstrip line is electrically small ($0.12\lambda_g$ being λ_g the equivalent wavelength at f=866MHz), the effect of the presence of the PCB board can not be neglected. Since the ETSI UHF RFID application is a narrowband application (percentage bandwidth of 0.35%), we can derive an equivalent circuit (Fig. 7) to deduct its effect and to compute a good approximation of the chip input impedance.

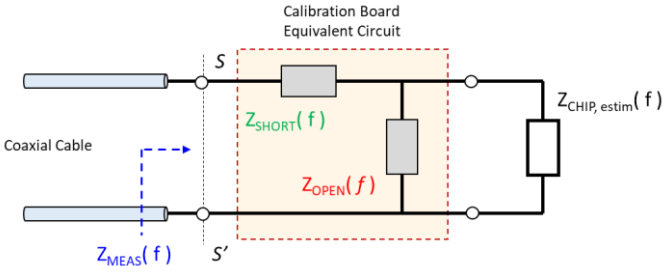

Fig. 7. Equivalent circuit considered for calibration procedure.

Specifically,

- Z_{MEAS} is the input impedance at the *SS'* section, the actual impedance measured by means of the VNA, when the chip is mounted on the PCB board (same layout of those used for calibration process and the chip is glued on it with a classical tin soldering process)
- Z_{SHORT} is the input impedance measured at *SS'* section when the RFID chip pads are short circuited (short termination). It is modeled as an in-series impedance (basically a series inductor), and it is considered independent on the temperature variation.

- Z_{OPEN} is the input impedance measured at *SS'* section when the microstrip line ends on an open termination. It is modeled as an in parallel impedance (basically a parallel capacitor), and it takes into account possible parasitic capacitive effects. It is considered independent on the temperature variation.

On the basis of this equivalent circuit, the chip input impedance has been estimated as a function of the frequency and by varying the temperature. Such an equivalent circuit is effective to derive a reliable chip input impedance estimation, at least in a narrowband around the ETSI UHF RFID central frequency (i.e. 866MHz). It is worth noting that the load termination is not considered to derive the equivalent circuit, but it has been used as a validation of the printed circuit.

The heating process was performed through the heating section of the Valp-ARE magnetic stirrer with a resolution of 5 °C. The tag temperature measured by means of standard RTD-ClassA-Pt100 glued with a thermal paste on the PCB and then connected to a Voltage-Imposed-Current-Monitor SMU, whose settings were imposed thanks to a PC controlled A-D/D-A interface (Fig. 8).

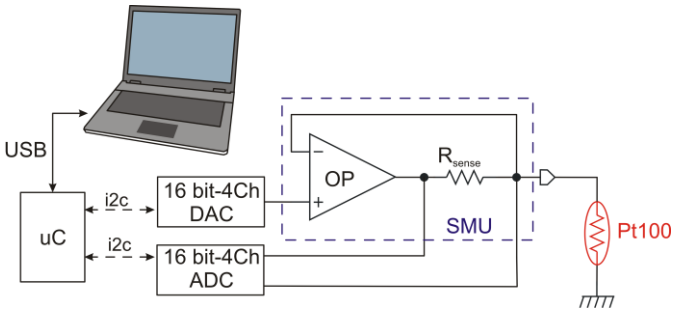

Fig. 8. Schematic block of the system used to measure the temperature by means of the RTD Pt100.

A Python-based software controls the DAC to impose the target voltage at the OP non-inverting input while the ADC converted the drop voltage across the R_{sense} and sent the value to the PC. After some simple algebraical manipulations of the collected values, it was possible to derive the value of the temperature. The value of R_{sense} was chosen equal to 100Ω. Other devices are: AD8647 operational amplifier, ADS1115 ADC, AD5665R DAC. By using the afore-described measurement setup, the chip input impedance was measured as a function of the frequency, for various values of temperature. In Fig. *9*, the real and imaginary parts of the measured chip input impedance as a function of both temperature and frequency are shown.

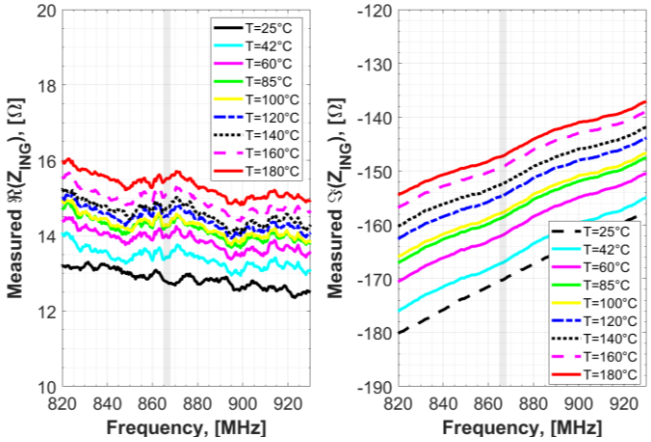

(a) (b)

Fig. 9. Measured (a) real and (b) imaginary part of the chip input impedance as a function of the frequency, for different values of temperature.

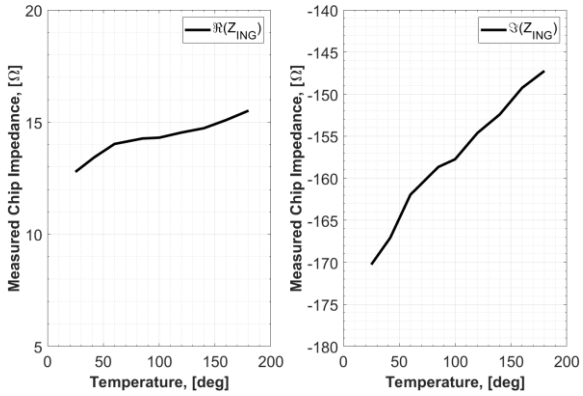

Fig. 10. Measured (a) real and (b) imaginary part of the chip input impedance as a function of the temperature, at a fixed frequency of 866 MHz.

In Fig. 10, both the real and imaginary part of the chip impedance are shown as a function of the temperature at a fixed frequency of 866 MHz. An increasing monotonical trend can be observed when increasing the temperature. The most significant variation is observed on the imaginary part of the measured impedance. The τ and *PRC* parameters were derived from the measurements by using equations (2) and (3), respectively. In Fig. 11, the *PRC* is depicted as a function of both temperature and frequency. Thus, the trend of both power transmission impedance and *PRC* are reported in Fig. 12 as a function of temperature, at the assigned frequency of 866MHz. In this case, the chip input impedance variation due to temperature leads to a shift of the resonance (i.e. minimum of *PRC*) toward lower frequencies. At frequencies close to 866MHz, the *PRC* factor assumes values lower than -10dB at room temperature, but it becomes higher than -3dB for temperature above 140°C, so significantly affecting the UHF RFID system performance. It is worth nothing that the resonance shift may be compensated by using an antenna with a wider bandwidth, which means a bigger size or a lower efficiency of the radiating element. In some specific scenarios neither of the two possibilities can be exploited due to strict mechanical and electromagnetic requirements.

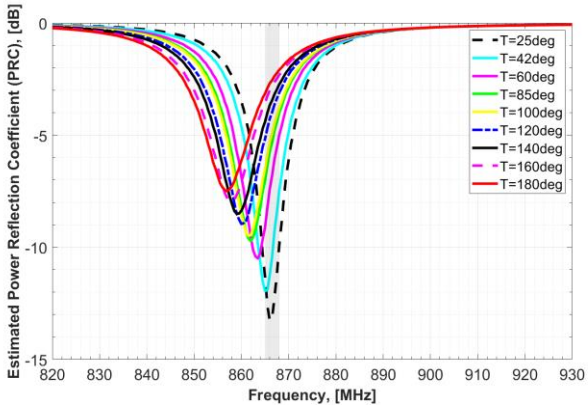

Fig. 11. Derived trend of PRC factor as function of the frequency, for different values of temperature.

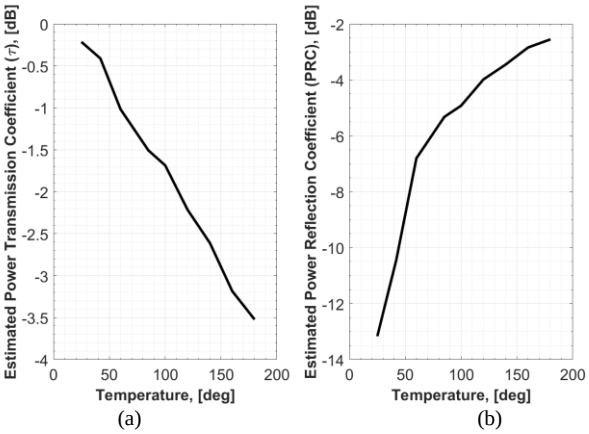

Fig. 12. Derived trend of (a) power transmission impedance (τ) and (b) Power Reflection Coefficient (PRC) as function of the temperature, at a fixed frequency of 866MHz.

B Effect of the Temperature on the Read Range

The effect of the temperature on the read range of the tag under test has been evaluated by using the measurement setup shown in Fig. 13a. A commercial circularly polarized UHF RFID antenna is placed at a distance *D* from the tag and connected to the commercial UHF RFID reader Impinj Speedway R420 [25] controlled by a laptop (Fig. 13a). Once again, the tag antenna was heated by the heating section of the Valp-ARE magnetic stirrer and the Pt100 was used to collect temperature values (Fig. 13b). Four tag-reader antenna distances have been considered: 30 cm, 50 cm, 70 cm and 90 cm. For a set of temperatures, ranging from 20 °C (room temperature) to 140 °C, the minimum power needed to activate the ceramic tag has been measured. As analysed in details in [26], the so-called tag sensitivity is an appropriate metric to jointly account for the chip and the antenna characteristics of the tag. It can be expressed as

$$S_{tag}(f,\theta,\phi) = \frac{S_{chip}}{\tau(f)\cdot G_{tag}(f,\theta,\phi)} \qquad (4)$$

where S_{chip} represents the chip sensitivity, τ represents the power transmission coefficient and G_{tag} represents the gain of the tag antenna. In this paper, system level performance analysis in terms of read range has been carried out at a fixed frequency of 866MHz and without varying the angles (θ, ϕ). However, we accounted for the temperature variation, thus the equation described in [26] can be re-written as

$$EIRP_{TX,ON} = \frac{S_{chip}(T)}{\tau(T)} \cdot \left(\frac{4\pi df}{c}\right)^2 \cdot \frac{1}{G_{tag}\cdot\eta_{plf}\cdot A_{cable}} \qquad (5)$$

where *c* is the light speed, η_{plf} is the polarization loss factor and A_{cable} is the attenuation introduced by the coaxial cable between the reader and the reader antenna. In a first analysis we assumed negligible the dependence of the temperature on the tag antenna gain, since the dilation of the copper layer can be ignored and the antenna is printed on a 1mm-thick alumina (Al_2O_3) substrate typically robust to high temperature. Moreover, the epoxy resin has been chosen to be robust to temperatures higher than 140°. On the other hand, it is not simple to predict the chip sensitivity variation under the effect of the temperature since it implies a detailed knowledge of the chip design. Hence, the activation Effective Isotropic Radiated Power ($EIRP_{TX,ON}$) is a function of the temperature, as described by equation (5). In Fig. 14, the activation Effective Isotropic Radiated Power ($EIRP_{TX,ON}$) is plotted as a function of the temperature, for the four considered distances. It can be noted that, for a fixed distance, the minimum reader output power needed to activate the tag increases if increasing the temperature of the tag (i.e. the chip), as expected due to the antenna-chip mismatch described in Section II.

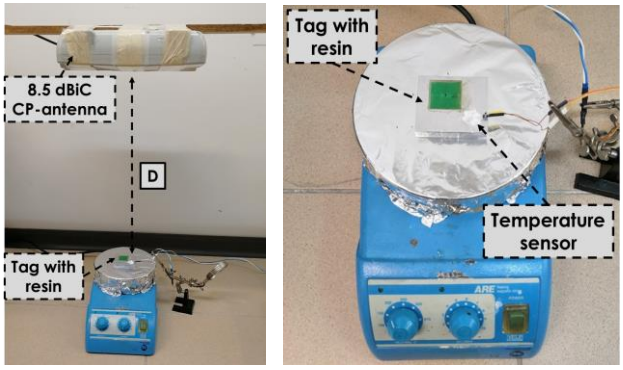

(a) (b)

Fig. 13. Pictures of the measurements setup: (a) CP antenna oriented towards tag on the magnetic stirrer. (b) Tag with temperature sensor (Pt100) connected on aluminium plate with thermal paste for temperature detection.

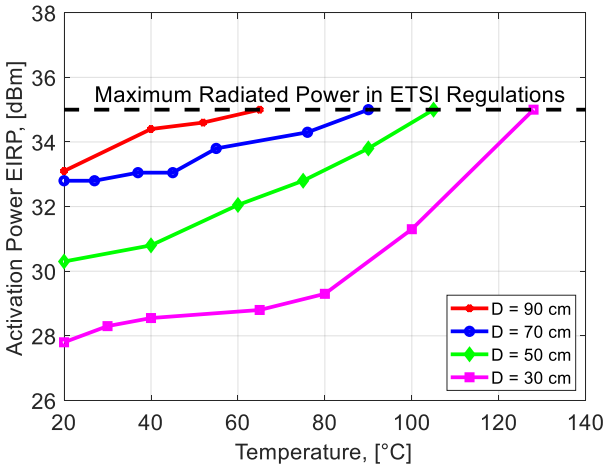

Fig. 14. Minimum EIRP needed to activate the ceramic tag placed at different distances, as a function of the temperature.

IV. Conclusion

The effect of the temperature on the overall UHF RFID system performance has been experimentally analysed. As a figure of merit, the Power Transmission Coefficient and the Power Reflection Coefficient have been considered. Specifically, after a proper calibration procedure performed with an ad-hoc calibration kit, the chip input impedance has been measured at a set of temperatures ranging from the room temperature up to 140 °C, highlighting its effect on the UHF RFID tag performance. Consequently, read range measurements have been performed while heating the ceramic tag antenna, confirming that high temperatures significantly affect the system behaviour, especially when the tag antennas are narrowband.

References

[1] K. Finkenzeller, *RFID Handbook: Fundamentals and Applications in Contactless Smart Cards and Identification*, 2nd ed. Hoboken, NJ: Wiley, 2003.

[2] A. Pratelli, M. Petri, A. Farina, and M. Lupi, “Improving Bicycle Mobility in Urban Areas Through ITS Technologies: The SaveMyBike Project”, Advanced Solutions of Transport Systems for Growing Mobility, Sierpiński G. (eds) TSTP 2017, Advances in Intelligent Systems and Computing, vol 631. Springer, Cham

[3] Y. S. Chang et al., "Development of RFID Enabled Aircraft Maintenance System," 2006 4th IEEE International Conference on Industrial Informatics, Singapore, 2006, pp. 224-229.

[4] S. Yang, M. Crisp, R. V. Penty and I. H. White, "RFID Enabled Health Monitoring System for Aircraft Landing Gear," in IEEE Journal of Radio Frequency Identification, vol. 2, no. 3, pp. 159-169, Sept. 2018.

[5] S. L. Chen, "A Miniature RFID Tag Antenna Design for Metal Objects Application," *IEEE Antennas and Wireless Propagation Letters*, vol. 8, pp. 1043-1045, 2009.

[6] S. L. Chen, K. H. Lin and R. Mittra, "A low profile RFID tag designed for metal objects," *Asia Pacific Microwave Conference*, Singapore, 2009, pp. 226-228.

[7] P. H. Yang, Y. Li, L. Jiang, W. C. Chew and T. T. Ye, "Compact Metal RFID Tag Antennas With a Loop-Fed Method," *IEEE Trans. on Antennas and Propagation*, vol. 59, no. 12, pp. 4454-4462, Dec. 2011.

[8] C. W. Moh, E. H. Lim, F. L. Bong and B. K. Chung, "Miniature Coplanar-Fed Folded Patch for Metal Mountable UHF RFID Tag," *IEEE Trans. on Antennas and Propagation*, vol. 66, no. 5, pp. 2245-2253, May 2018.

[9] F. L. Bong, E. H. Lim and F. L. Lo, "Flexible Folded-Patch Antenna With Serrated Edges for Metal-Mountable UHF RFID Tag," *IEEE Trans. on Antennas and Propagation*, vol. 65, no. 2, pp. 873-877, Feb. 2017.

[10] A. A. Babar, T. Bjorninen, V. A. Bhagavati, L. Sydanheimo, P. Kallio and L. Ukkonen, "Small and Flexible Metal Mountable Passive UHF RFID Tag on High-Dielectric Polymer-Ceramic Composite Substrate," *IEEE Antennas and Wireless Propagation Letters*, vol. 11, pp. 1319-1322, 2012.

[11] K. Jaakkola, "Small On-Metal UHF RFID Transponder With Long Read Range," *IEEE Trans. on Antennas and Propagation*, vol. 64, no. 11, pp. 4859-4867, Nov. 2016.

[12] K. Jaakkola and P. Koivu, "Low-Cost and Low-Profile Near Field UHF RFID Transponder for Tagging Batteries and Other Metal Objects," *IEEE Trans. on Antennas and Propagation*, vol. 63, no. 2, pp. 692-702, Feb. 2015.

[13] A. Michel, V. Franchina, P. Nepa and A. Salvatore, "A UHF RFID Tag Embeddable in Small Metal Cavities," in *IEEE Transactions on Antennas and Propagation*, vol. 67, no. 2, pp. 1374-1379, Feb. 2019.

[14] V. Franchina, A. Michel, P. Nepa and A. Salvatore, "Compact In-metal UHF RFID Tag for Manufactured Metallic Components," *2018 3rd International Conference on Smart and Sustainable Technologies (SpliTech)*, Split, 2018, pp. 1-5.

[15] V. Franchina, A. Ria, A. Michel, P Bruschi, P. Nepa and A. Salvatore, " A Compact UHF RFID Ceramic Tag for High-Temperature Applications," *2019 IEEE International Conference on RFID Technology and Applications (RFID-TA)*, Italy, 2019.

[16] S. Lahokallio, J. Kiilunen and L. Frisk, "Performance of passive RFID tags in a high temperature cycling test," *Proceedings of the 5th Electronics System-integration Technology Conference (ESTC)*, Helsinki, 2014, pp. 1-5.

[17] C. Occhiuzzi, S. Amendola, S. Nappi, N. D'Uva and G. Marrocco, "Sensing-oriented RFID tag Response in High Temperature Conditions," *2018 3rd International Conference on Smart and Sustainable Technologies (SpliTech)*, Split, 2018, pp. 1-4.

[18] A. Gutierrez *et al*., "High-frequency RFID tag survivability in harsh environments," *2013 IEEE International Conference on RFID (RFID)*, Penang, 2013, pp. 58-65.

[19] X. Yu, Y. Yu, D. Wang, K. Qian, J. Liu and Z. Zhao, "A Novel Temperature Control System of Measuring the Dynamic UHF RFID Reading Performance," *2016 Sixth International Conference on Instrumentation & Measurement, Computer, Communication and Control (IMCCC)*, Harbin, 2016, pp. 322-326.

[20] Epoxy resin, http://www.lookpolymers.com/pdf/Master-Bond-EP46HT-Epoxy-Adhesive-for-Structural-Bonding.pdf

[21] Alien Technology, Higgs®4 chip datasheet http://www.alientechnology.com/products/ic/higgs-4/

[22] V. Franchina, A. Michel, P. Nepa and A. Salvatore, "Compact In-metal UHF RFID Tag for Manufactured Metallic Components," *2018 3rd International Conference on Smart and Sustainable Technologies* (SpliTech), Split, 2018, pp. 1-5.

[23] A. Ghiotto, S. F. Cantalice, T. P. Vuong, A. Pouzin, G. Fontgalland and S. Tedjini, "Miniaturized patch antenna for the Radio Frequency Identification of metallic objects," *2008 IEEE MTT-S International Microwave Symposium Diges*t, Atlanta, GA, USA, 2008, pp. 583-586.

[24] M. B. Eunni, "A Novel Planar Microstrip Antenna Design for UHF RFID," M.S. thesis, Madras University, India, May 2004.

[25] RFID Reader Impinj Speedway R420, https://www.impinj.com/platform/connectivity/speedway-r420/

[26] R. Colella, L. Catarinucci, P. Coppola and L. Tarricone, "Measurement Platform for Electromagnetic Characterization and Performance Evaluation of UHF RFID Tags," in IEEE Transactions on Instrumentation and Measurement, vol. 65, no. 4, pp. 905-914, April 2016.